Transition from partly standing to progressive internal tides in Monterey Submarine Canyon

Rob A. Hall[a,*], Matthew H. Alford[b], Glenn S. Carter[c], Michael C. Gregg[b], Ren-Chieh Lien[b], Danielle J. Wain[d], Zhongxiang Zhao[b]

[a]*School of Environmental Sciences, University of East Anglia, Norwich Research Park, Norwich, NR4 7TJ, UK*
[b]*Applied Physics Laboratory, University of Washington, 1013 NE 40th Street, Seattle, WA 98105, USA*
[c]*Department of Oceanography, University of Hawai'i at Mānoa, Marine Science Building, 1000 Pope Road, Honolulu, HI 96822, USA*
[d]*Department of Architecture and Civil Engineering, University of Bath, Claverton Down, Bath, BA2 7AY, UK*

Abstract

Monterey Submarine Canyon is a large, sinuous canyon off the coast of California, the upper reaches of which were the subject of an internal tide observational program using moored profilers and upward-looking moored ADCPs. The mooring observations measured a near-surface stratification change in the upper canyon, likely caused by a seasonal shift in the prevailing wind that favoured coastal upwelling. This change in near-surface stratification caused a transition in the behaviour of the internal tide in the upper canyon from a partly standing wave during pre-upwelling conditions to a progressive wave during upwelling conditions. Using a numerical model, we present evidence that either a partly standing or a progressive internal tide can be simulated in the canyon, simply by changing the initial stratification conditions in accordance with the observations. The mechanism driving the transition is a dependence of down-canyon (supercritical) internal tide reflection from the canyon floor and walls on the depth of maximum stratification. During pre-upwelling conditions, the main pycnocline extends down to 200 m (below the canyon rim) resulting in increased supercritical reflection of the up-canyon propagating internal tide back down the canyon. The large up-canyon and smaller down-canyon progressive waves are the two components of the partly standing wave. During upwelling conditions, the pycnocline shallows to the upper 50 m of the watercolumn (above the canyon rim) resulting in decreased supercritical reflection and allowing the up-canyon progressive wave to dominate.

Keywords: Internal waves, Internal tides, Submarine canyons, USA, California, Monterey Bay

1. Introduction

Monterey Submarine Canyon (MSC) is a large, sinuous canyon situated in Monterey Bay, California. It is the largest submarine canyon along the west coast of the United States and has been the focus of several internal tide observational programs (Key, 1999; Kunze et al., 2002; Johnston et al., 2011; Kunze et al., 2012) and numerical modelling studies (Petruncio et al., 2002; Jachec et al., 2006; Wang et al., 2009; Kang and Fringer, 2012). In stratified seas, barotropic (surface) tidal flow across the sloping topography typical of submarine canyons can generate internal tides (internal gravity waves with tidal frequencies) by vertically displacing density surfaces (Bell, 1975; Baines, 1982). Submarine canyons are also thought to trap internal waves and internal tides originating outside the canyon, through reflection from the sloping topography, and channel the energy towards the canyon floor (Gordon and Marshall, 1976) and canyon head (Hotchkiss and Wunsch, 1982). Elevated internal wave energy near the canyon floor and head has been observed in several submarine canyons worldwide (e.g., Wunsch and Webb, 1979; Hotchkiss and Wunsch, 1982; Wang et al., 2008; Lee et al., 2009) and the mechanism is thought to be responsible for high turbulent mixing rates measured near the head of MSC (Lueck and Osborn, 1985; Carter and Gregg, 2002).

MSC is a "Type-2" canyon (Harris and Whiteway, 2011) in that it incises the continental shelf but does not connect to a major river. It extends over 100 km, from the abyssal plain at the base of the continental slope, to within 100 m of Moss Landing in the centre of the Monterey Bay. The bathymetry of MSC is complex, featuring a pair of large meanders (San Gregorio and Monterey Meanders) near the mouth of the bay and a smaller meander (Gooseneck Meander) closer to the canyon head (Fig. 1a,b). In the upper reaches, the canyon rim is $\sim$ 100 m deep, increasing to roughly 200 m near the canyon mouth.

The first quantitative measurements of internal tides in MSC were made in April and October 1994 during two "Internal Tide Experiments" (ITEX1 and ITEX2, Petruncio et al., 1998) and focused on the region between Gooseneck Meander and the canyon head. One of the key findings was an apparent change in the behaviour of the internal

*Corresponding author
Email address: robert.hall@uea.ac.uk (Rob A. Hall)

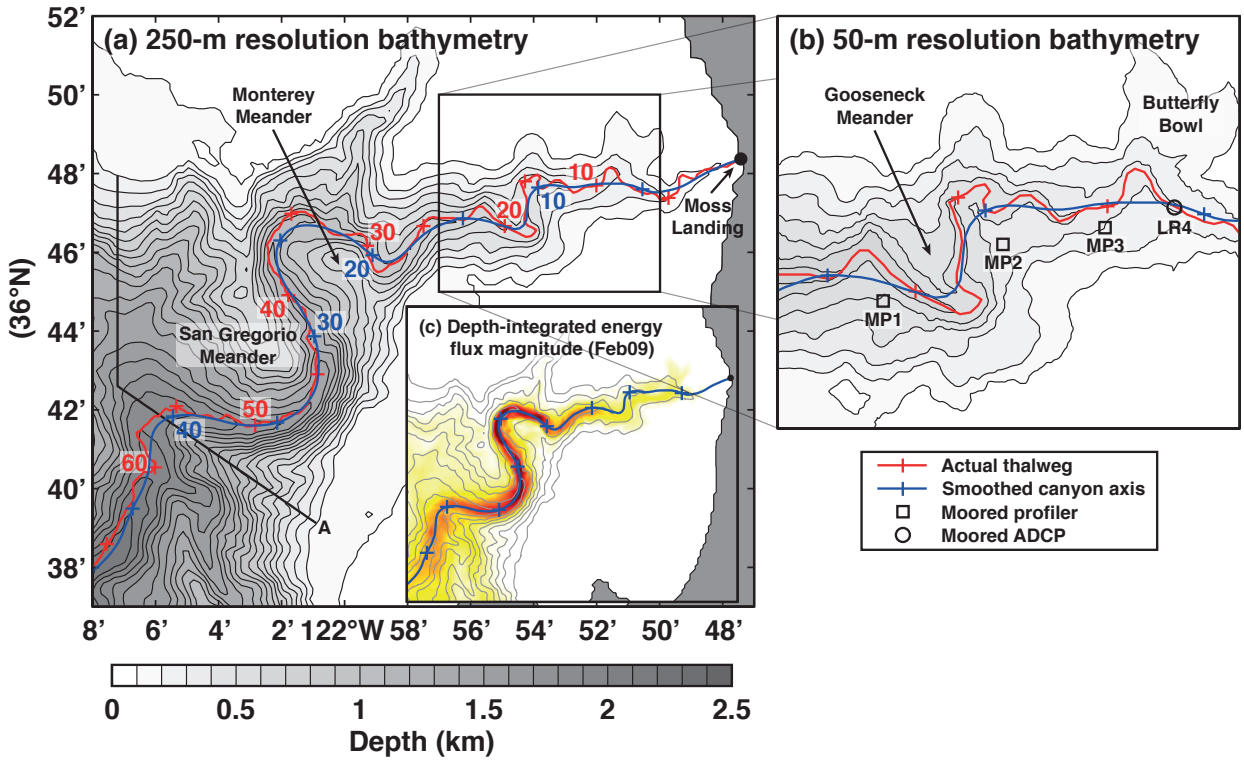

Figure 1: (a) Model bathymetry of Monterey Submarine Canyon. (b) High-resolution bathymetry of the upper canyon showing the locations of the moored profilers and moored ADCP. The contour interval is 100 m. The red and blue lines are the actual thalweg and smoothed canyon axis respectively. For both canyon axes, along-canyon distance from Moss Landing is marked with a cross at 5-km intervals. (c) Depth-integrated baroclinic M_2 energy flux magnitude in the canyon region for the *Feb09* model run.

tide from an up-canyon propagating progressive wave during April (ITEX1) to a horizontally standing wave during October (ITEX2). Petruncio et al. (1998) attributed the change in behaviour to an increase in stratification between the two experiment periods and down-canyon reflection of the internal tide from bathymetry near the canyon head during ITEX2.

In a more recent experiment ("Internal Tide and Mixing in Monterey and Ascension Canyons"), Zhao et al. (2012) observed a change in the behaviour of the internal tide in the upper reaches of MSC from a partly standing wave during February 2009 to a progressive wave during late March/April 2009. Details of this experiment are given in Section 1.2. Further observational evidence of a progressive internal tide during April 2009 was presented by Wain et al. (Submitted).

Numerical modelling studies of internal tides in the MSC region (Jachec et al., 2006; Carter, 2010; Hall and Carter, 2011; Kang and Fringer, 2012) have shown that the internal tide observed in the canyon is likely generated on Sur Slope, roughly 40 km to the south of the canyon mouth. Hall and Carter (2011) presented evidence that more remote generation sites in the region, including two offshore seamounts, have only a minor influence on the internal tide in the canyon.

1.1. Standing and partly standing internal waves

Standing internal waves are the superposition of two equal-amplitude progressive internal waves propagating in opposite directions, as described by Petruncio et al. (1998) and Nash et al. (2004, 2006). For a perfectly standing mode-1 internal wave over a flat bottom, the horizontal energy flux parallel to the axis of wave propagation is zero, but, the horizontal energy flux perpendicular to the axis is non-zero and varies sinusoidally. This transverse energy flux has maxima and minima distributed every $\lambda/4$, where λ is the horizontal wavelength of the component progressive waves. Horizontal kinetic energy (HKE) and available potential energy (APE) also vary sinusoidally along the axis of wave propagation, but are out of phase such that the HKE/APE ratio goes from zero to ∞ at $\lambda/4$ intervals. If the standing wave is setup by reflection from a vertical boundary, the transverse energy flux and HKE/APE ratio are zero at the boundary.

Partly standing internal waves occur when the component progressive internal waves have unequal amplitudes. The mode-1 standing internal wave energy equations were generalised to include partly standing waves by Martini et al. (2007). For a partly standing mode-1 internal wave, the parallel energy flux is uniform and in the direction of the major (i.e., largest amplitude) component wave. Like a perfectly standing wave, the transverse energy flux, HKE,

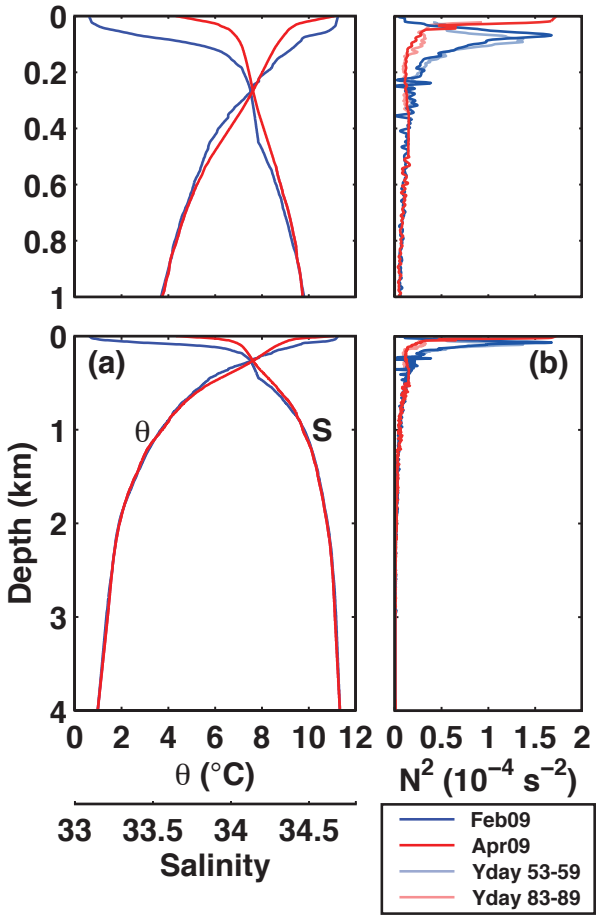

Figure 2: (a) Potential temperature and salinity profiles used to set the initial stratification for the two model runs (blue: *Feb09*, red: *Apr09*). (b) Corresponding N^2 profiles. The upper panels are expansions of the upper 1 km to highlight the near-surface differences. The light blue and light red lines are representative N^2 profiles for the two parts of the observational period, calculated as 6-day time-averages of temperature/salinity profiles from moored profiler MP2.

and APE all vary sinusoidally along the axis of wave propagation; the locations of the maxima and minima are determined by the relative phases of the component waves. The range of HKE/APE decreases from ∞ as the amplitude difference between the component waves increases.

If the amplitude of one of the component waves goes to zero, the result is a purely progressive internal wave. Parallel energy flux is uniform and in the direction of wave propagation; transverse energy flux goes to zero; and both HKE and APE are uniform. HKE/APE goes to $(\omega^2 + f^2)/(\omega^2 - f^2)$ (Gill, 1982), where ω is the angular frequency of the wave and f is the inertial frequency.

1.2. Mooring observations

Three McLane Moored Profilers (MP1, MP2, and MP3) and four moorings with upward-looking 75-kHz Acoustic Doppler Current Profilers (ADCPs) were deployed in the upper reaches of MSC between February and April 2009. The moored profilers measured near-full-depth vertical profiles of temperature, salinity, and current velocity; allowing the calculation of internal tide energy fluxes. One ADCP mooring (LR4) included a chain of nine temperature loggers to allow a similar calculation. The locations of the moored profilers and LR4 are shown in Fig. 1b. Most of the instruments recorded from approximately yearday[1] 48 to 106, with the exception of MP1 which failed on yearday 59. Full details of the mooring deployments and data analysis can be found in Zhao et al. (2012).

The mooring observations measured a near-surface stratification change in the upper canyon during early March 2009 (yearday 65-70), likely caused by a seasonal shift in the prevailing wind that favoured coastal upwelling (Zhao et al., 2012). During pre-upwelling conditions, the main pycnocline extended from 50 m down to 200 m (Fig. 2b, Yday 53-59), below the canyon rim. During upwelling conditions, the pycnocline shallowed to the upper 50 m of the watercolumn (Fig. 2b, Yday 83-89), above the canyon rim.

Zhao et al. (2012) suggested this change in near-surface stratification caused a transition in the behaviour of the internal tide in the upper canyon from a partly standing wave during pre-upwelling conditions to a progressive wave during upwelling conditions (Fig. 3). Evidence for the transition includes: (a) change in the mode-1 HKE/APE ratio at MP2 from less than one during pre-upwelling conditions to around the theoretical value for a progressive internal wave, $(\omega^2 + f^2)/(\omega^2 - f^2) \approx 2.2$, during upwelling conditions. (b) Change in the observed mode-1 group speed from less than half the theoretical mode-1 group speed pre-upwelling to approximately equal the theoretical group speed during upwelling. (c) Mode-1 M_2 displacement at the four mooring sites being in-phase pre-upwelling but phase-lagged in the up-canyon direction during upwelling.

1.3. Numerical modelling

Despite this convincing evidence that a partly standing internal tide existed in the upper canyon during the pre-upwelling part of the observational period, numerical modelling studies have failed to diagnose standing or partly standing wave behaviour. Carter (2010) and Hall and Carter (2011) used a regional model with stratification representative of pre-upwelling conditions to investigate the surface and internal tides in the canyon region. However, the focus of these studies was the broader scale distribution of tidal energy and little attention was payed to the canyon head region. Although Hall and Carter (2011) speculated that partly standing waves may be responsible for areas of elevated APE relative to HKE in the canyon, they conceded that the meandering bathymetry complicated the analysis and no coherent pattern consistent with a partly standing wave was found.

[1]We refer to time using yearday, defined as decimal days since midnight on 31 December 2008 (e.g., noon on 31 January 2009 is yearday 30.5).

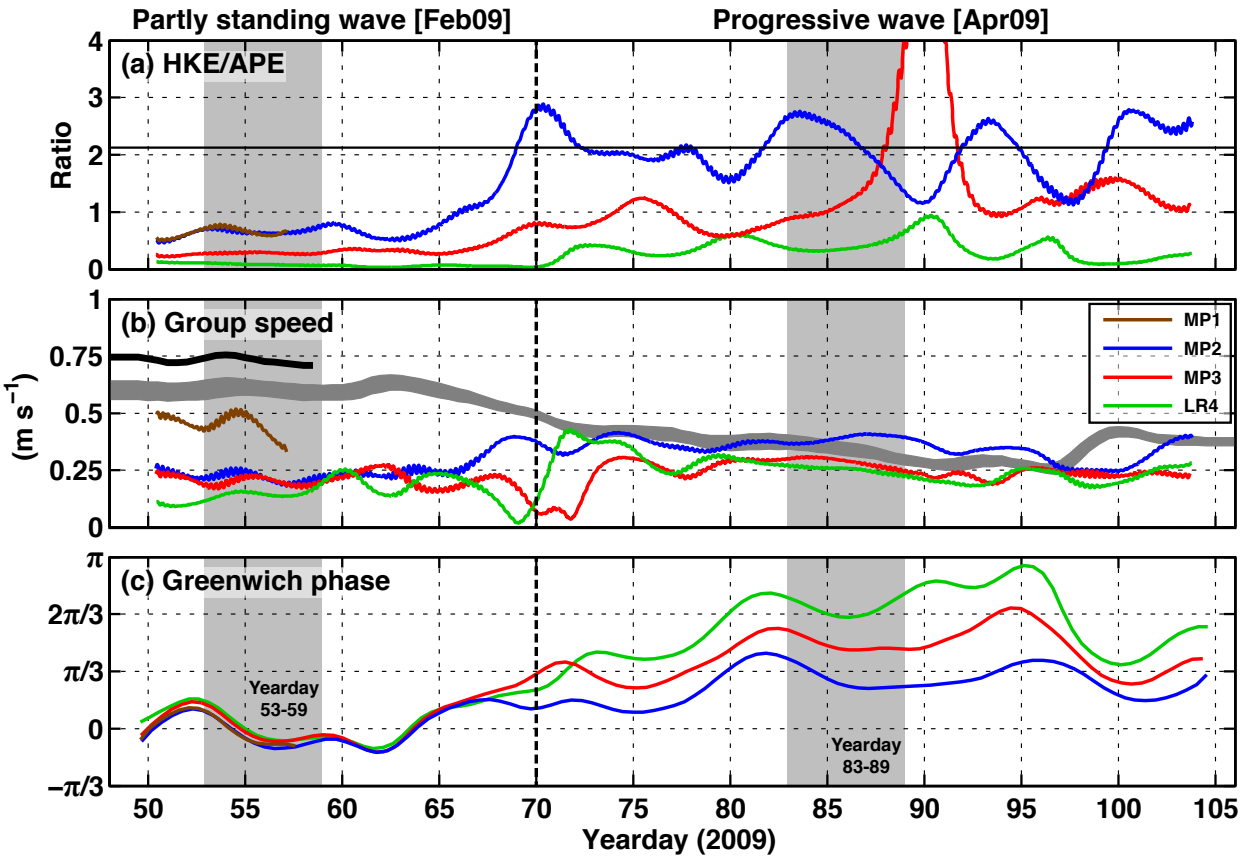

Figure 3: Mode-1 semidiurnal partly standing and progressive internal tides, diagnosed from the moored profilers and moored ADCP. (a) HKE/APE ratio. The horizontal black line is the theoretical value for a progressive internal wave, ~ 2.2. (b) Observed group speed (coloured lines) and theoretical mode-1 group speed (black line: MP1, grey band: MP2, MP3, and LR4). (c) Greenwich phase of mode-1 M_2 displacement. The thick dashed line indicates the transition from partly standing to progressive internal tides and the shaded areas are representative days for the two regimes. Figure adapted from Zhao et al. (2012).

Here, we re-examine the results of Hall and Carter (2011) by interpolating the model output onto a smoothed canyon axis that removes the influence of small-scale meanders. The results are compared with a new model simulation using stratification representative of upwelling conditions. Both model runs support the observational evidence that the internal tide transitions from a partly standing wave to a progressive wave as the main pycnocline shallows. We then expand on the analysis of Petruncio et al. (1998) and Zhao et al. (2012) to identify likely areas of internal tide reflection near the canyon head and propose a mechanism by which a small change in the depth of the pycnocline, if moved from below to above the canyon rim, can have a dramatic effect on internal tide dynamics.

2. Numerical model setup

A modified version of the Princeton Ocean Model (POM, Blumberg and Mellor, 1987) is used to simulate partly standing and progressive M_2 internal tides in MSC. POM is a three-dimensional, nonlinear, hydrostatic, free-surface, finite-difference, terrain-following (σ coordinate), primitive equation model. The Flather condition (Flather, 1976) is applied at the boundaries so that barotropic energy is transmitted out of the domain. Baroclinic energy is absorbed at the boundaries using the relaxation scheme described by Carter and Merrifield (2007).

The model domain is the same as used by Carter (2010), Hall and Carter (2011), and Gregg et al. (2011). It extends from 123° 43′ 59″W, 35° 31′ 13″N to 121° 44′ 8″W, 37° 9′ 50″N with 250-m horizontal resolution; the bathymetry is derived from Monterey Bay Aquarium Research Institute multibeam data. The full model domain is shown in Fig. 1 of Carter (2010) and includes several internal tide generation sites, including Sur Slope and two offshore seamounts. Fifty-one evenly spaced sigma levels are used, giving vertical resolution between 0.3 m and 80 m depending on the total depth.

Initial conditions are no flow and horizontally uniform stratification. Two model simulations are compared, with different temperature/salinity profiles used to set the initial stratification (Fig. 2a). The first, denoted *Feb09*, represents pre-upwelling conditions and is the average of seven CTD casts at 123° 00′ 00″W, 36° 36′ 30″N taken over

12 h on yearday 48-49. The second stratification profile (*Apr09*) represents upwelling conditions and is the average of six CTD casts at the same location taken over 12 h on yearday 94. To better represent the near-surface stratification in the upper canyon during the upwelling part of the observational period, time-averaged temperature/salinity profiles from moored profiler MP2 (121° 53′ 24″W, 36° 47′ 13″N; yearday 80-106) are used for the upper 500 m of *Apr09*. Linear extrapolation is used to extend both profiles from 3000 m to 4000 m. The corresponding profiles of buoyancy frequency squared (N^2) are in good agreement with moored profiler observations in the upper canyon (Fig. 2b).

Both model simulations are forced at the boundaries with M_2 barotropic velocities. Elevations and normal velocities used to calculate the Flather boundary condition are taken from the TPXO6.2 inverse model (Egbert, 1997; Egbert and Erofeeva, 2002).

Surface buoyancy and momentum fluxes are set to zero. Diffusivities are not applied to the temperature and salinity fields so the stratification is not eroded by mixing in the absence of a restoring buoyancy flux. M_2 is the dominant tidal constituent in the region and single-constituent forcing, combined with non-evolving stratification, allows rapid model spin-up and simplified analysis. The simulations are run for 20 M_2 tidal cycles (10.35 days) and M_2 harmonic analyses performed over the last six cycles.

3. Model diagnostics

3.1. Internal tide energetics

Baroclinic energy flux and baroclinic energy densities are calculated from the harmonic analyses output. Internal (baroclinic) tide energy flux is calculated as

$$\mathbf{F} = \langle \mathbf{u}' p' \rangle \,, \tag{1}$$

where $\mathbf{u}'$ is the velocity perturbation, p' is the pressure perturbation, and $\langle \cdot \rangle$ denotes an average over a tidal cycle (e.g., Kunze et al., 2002; Nash et al., 2005). The perturbations $\mathbf{u}'$ and p' are reconstructed from the harmonic constants. HKE and APE densities are calculated as

$$\text{HKE} = \frac{1}{4}\rho(u_A^2 + v_A^2), \tag{2}$$

$$\text{APE} = \frac{1}{4}\rho N^2 \xi_A^2, \tag{3}$$

where u_A and v_A are the baroclinic horizontal velocity amplitudes and ξ_A is the vertical displacement amplitude (inferred from vertical velocity amplitude).

Following Alford and Zhao (2007), internal tide group speed is calculated $c_g = |\widehat{\mathbf{F}}|/\widehat{E}$, where E is total baroclinic energy density ($E = \text{HKE} + \text{APE}$) and $\widehat{\cdot}$ denotes a depth-integral.

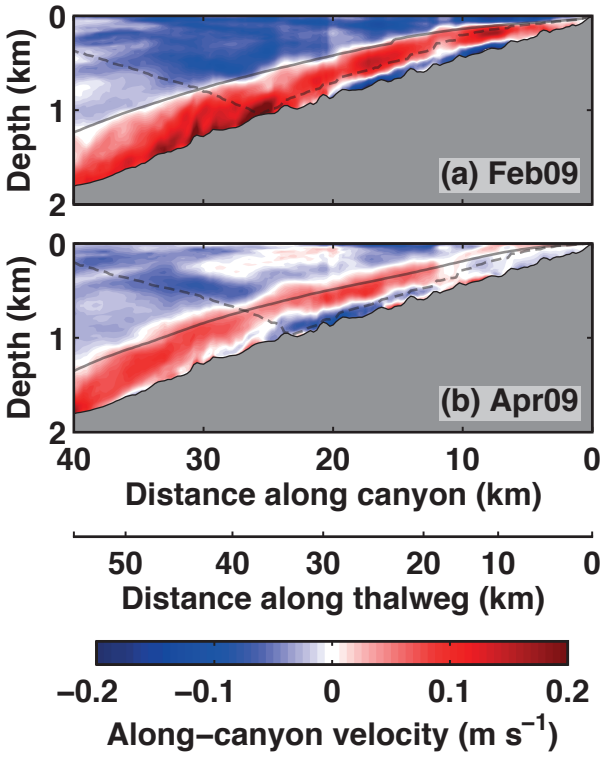

Figure 4: Along-canyon baroclinic M_2 velocity with distance along the canyon at high water for (a) *Feb09* and (b) *Apr09*. Positive values are towards the canyon head. The second horizontal axis is approximate distance along the actual thalweg. The solid (dashed) grey lines are M_2 internal tide characteristics following the smoothed canyon axis (actual thalweg).

3.2. Definition of "along-canyon"

Many previous studies of MSC have identified bathymetric features by their along-canyon distance from the canyon head. Hall and Carter (2011), Zhao et al. (2012), and Wain et al. (Submitted) used distance from Moss Landing along the canyon axis (thalweg[2]), calculated from high-resolution (50 m) bathymetry. In the upper canyon, the thalweg features small-scale (< 2 km) meanders that appear not to influence the path of the internal tide. As a result, along-thalweg distance is not an ideal reference frame in which to interpret internal tide observations and model simulations.

Guided by the modelling results of Hall and Carter (2011), we define a smoothed canyon axis that better follows the path of the depth-integrated baroclinic M_2 energy flux (Fig. 1c). This new along-canyon path is calculated by applying a 11-point running mean to the location of the thalweg in the model bathymetry (250-m resolution). The length of the smoothing window (2.5 km) is comparable to the canyon width in the upper reaches

[2]The thalweg of a canyon is the line that connects the deepest points of a series of bathymetric cross-sections along the length of the canyon. Higher resolution bathymetry will tend to result in a longer thalweg because smaller scale meanders are resolved.

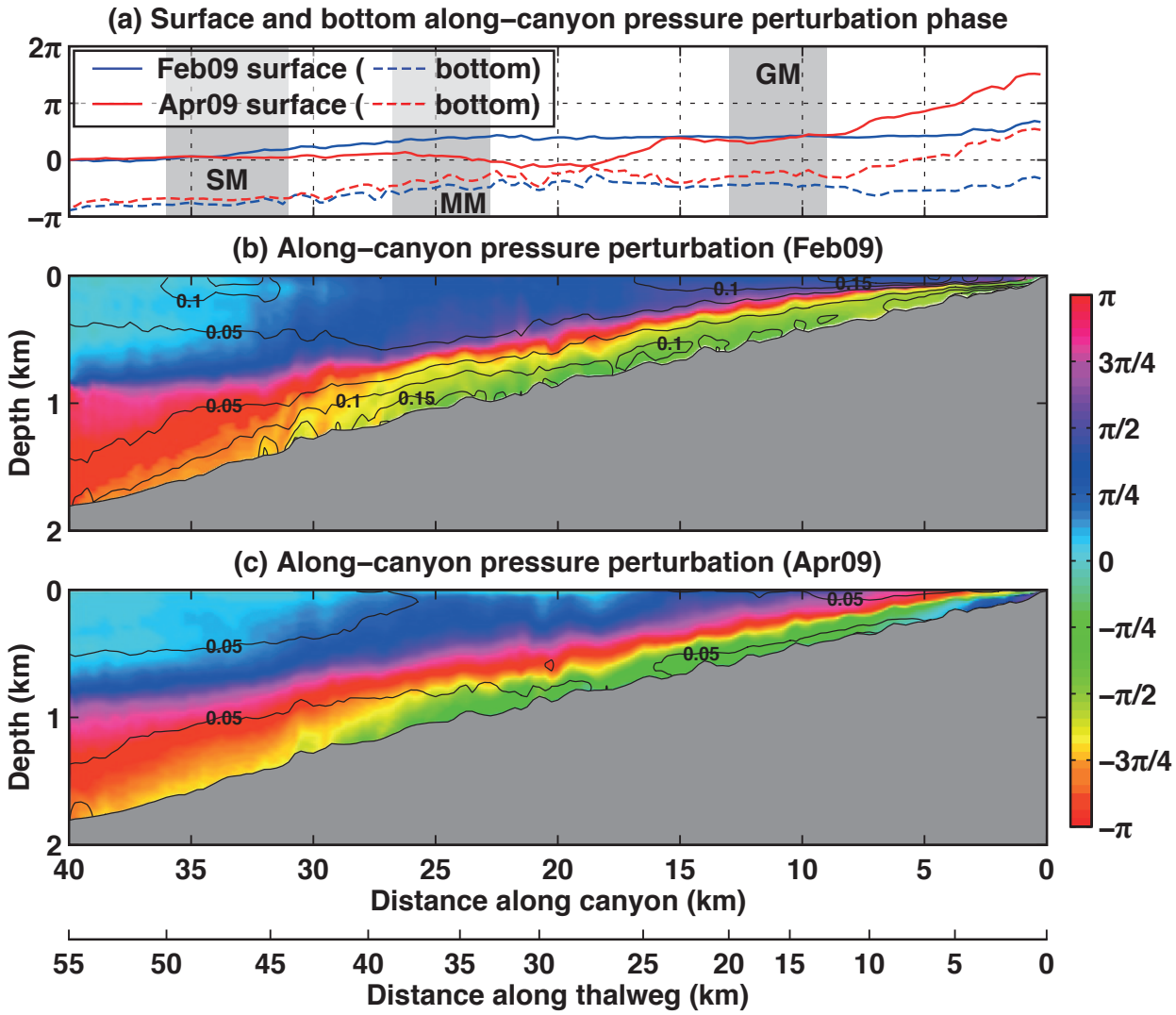

Figure 5: (a) Surface and bottom M_2 pressure perturbation phase with distance along the canyon for *Feb09* (blue) and *Apr09* (red). The shaded areas are the locations of the meanders. M_2 pressure perturbation phase (colour) and amplitude (black contours) with distance along the canyon for (b) *Feb09* and (c) *Apr09*. The pressure amplitude contour interval is 0.05 Pa.

but short compared to the mode-1 horizontal wavelength of a M_2 internal tide (order 30 km at Gooseneck Meander). Between the canyon head and Monterey Meander, distance along the smoothed canyon axis is up to 35% shorter than along-thalweg distance (Fig. 1a). However, around Monterey and San Gregorio Meanders, the relationship between along-canyon distance and along-thalweg distance is roughly uniform ($\sim 30\%$) due to the dominance of larger scale bathymetric features. In this study, all "along-canyon" figures and distances follow the smoothed canyon axis.

To confirm that the smoothed canyon axis well represents the path of the internal tide, baroclinc M_2 velocity along the smoothed axis at high water is shown in Fig. 4. For both stratifications, the slope of the near-bottom internal tide beam is in good agreement with the slope of M_2 internal tide characteristics (Fig. 4, solid lines), calculated from the internal wave dispersion relation,

$$s_{\text{wave}} = \sqrt{\frac{\omega^2 - f^2}{N^2 - \omega^2}}. \tag{4}$$

Internal tide characteristics calculated using along-thalweg distance rather than along-canyon (Fig. 4, dashed lines) are steeper than the near-bottom internal tide beam.

4. Effect of stratification on internal tide propagation

The two model simulations with different stratifications represent the partly standing (*Feb09*) and progressive (*Apr09*) internal tide regimes in MSC. Model evidence that the internal tide transitions from a partly standing wave to a progressive wave as the main pycnocline shallows is laid out in the following four subsections.

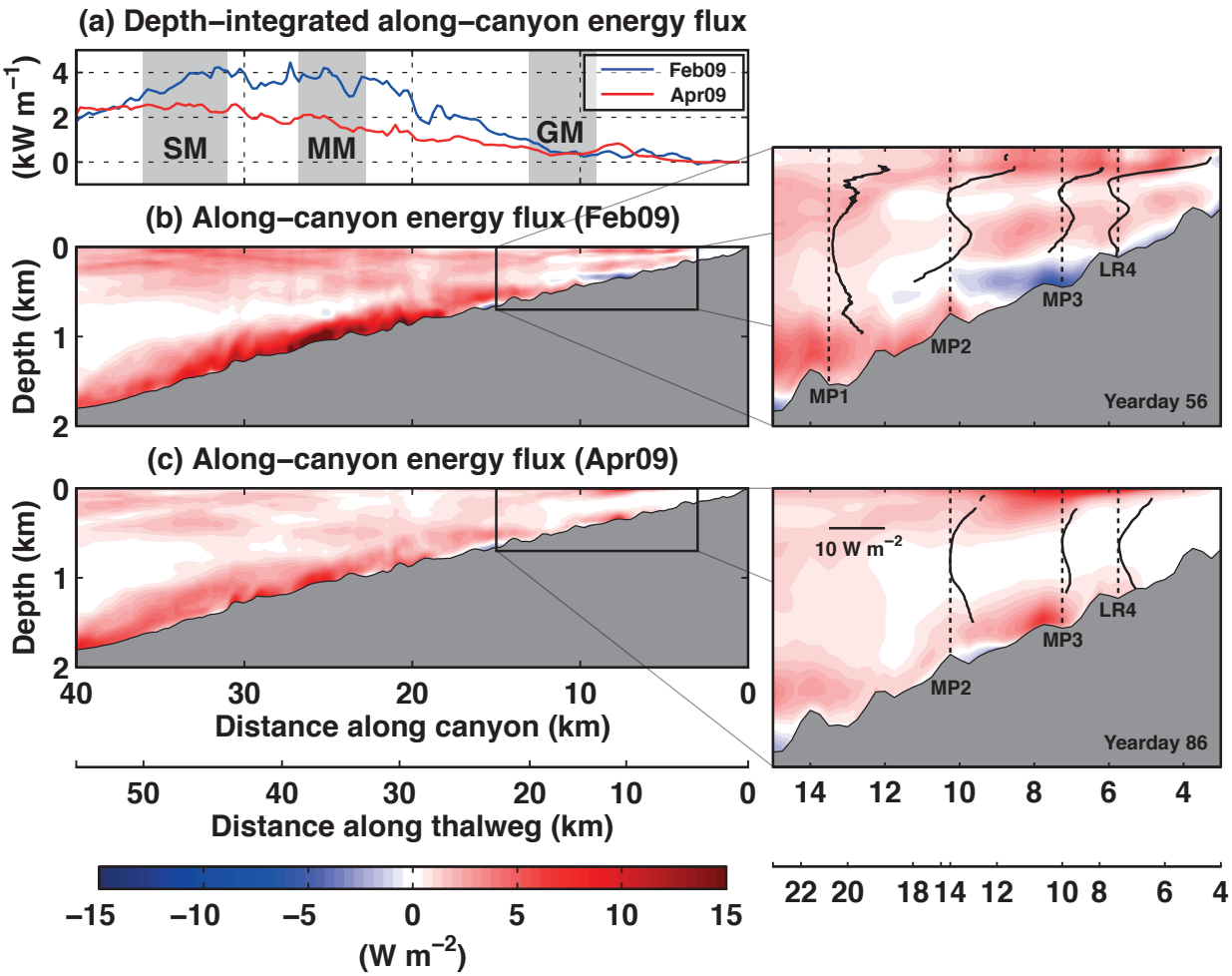

Figure 6: (a) Depth-integrated along-canyon baroclinic M_2 energy flux with distance along the canyon for *Feb09* (blue) and *Apr09* (red). The shaded areas are the locations of the meanders. Along-canyon baroclinic M_2 energy flux with distance along the canyon for (b) *Feb09* and (c) *Apr09*. Positive values are towards the canyon head. The region of the upper canyon where the moorings were located is expanded in the panels on the right. The black lines are vertical profiles of along-canyon baroclinic semidiurnal energy flux from the mooring observations on yearday 56 and 86 (positive values right of the dashed lines).

4.1. Along-canyon pressure perturbation

Arguably, the most convincing evidence that a partly standing internal tide existed in the upper canyon during the pre-upwelling part of the observational period is that mode-1 M_2 displacement is in-phase at all four of the mooring sites (Fig. 3c). To investigate the same effect in the model simulations, the phase and amplitude of pressure perturbation along the smoothed canyon axis are shown in Fig. 5. The phases are adjusted so that pressure perturbation phase is zero at the surface, 40 km from the canyon head for both stratifications.

For *Feb09* (Fig. 5b), there is little along-canyon change in pressure perturbation phase between 25 km and the canyon head. This spatially uniform phase is most evident at the surface and bottom (Fig. 5a, blue lines) and suggests a (partly) standing wave between Monterey Meander and the canyon head. For *Apr09* (Fig. 5c), there is an increase in pressure perturbation phase up-canyon, between 10 km and the canyon head, at both the surface and the bottom (Fig. 5a, red lines). This phase-lag suggests a progressive wave propagating up-canyon between Gooseneck Meander and the canyon head.

The total phase-lag between 40 km (canyon mouth) and the canyon head is 4.5 rad for *Apr09*, compared with 6.0 rad for a theoretical mode-1 M_2 internal tide with *Apr09* stratification (based on a canyon-average group speed of 0.94 m s^{-1}). The modelled internal tide therefore propagates at $\sim$ 76% progressive wave phase speed. In comparison, the *Feb09* internal tide propagates at only 38% progressive wave phase speed.

4.2. Along-canyon energy flux

Baroclinic M_2 energy flux along the smoothed canyon axis (Fig. 6b,c) is more coherent than along the actual thalweg (e.g., Fig. 6 of Hall and Carter, 2011) because the new along-canyon direction is better orientated with

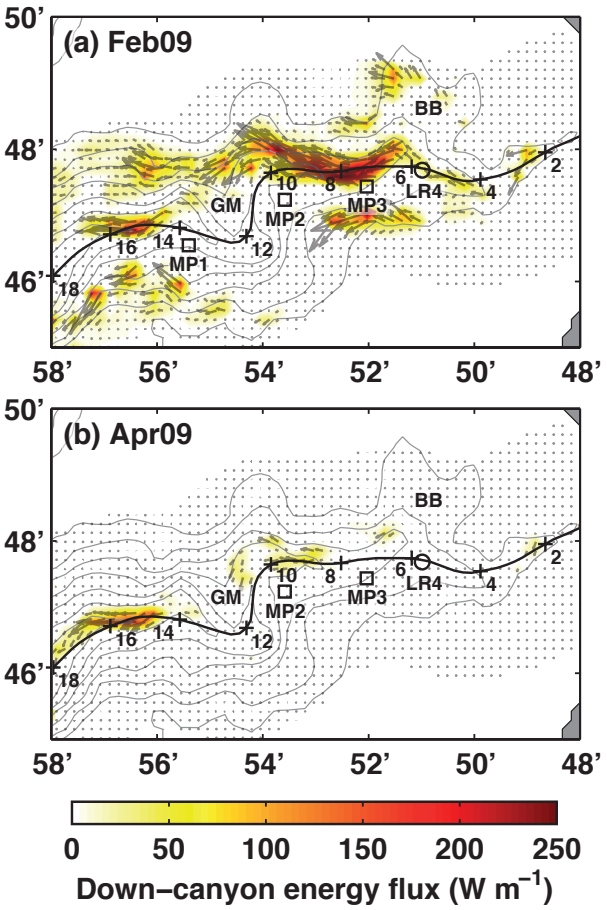

Figure 7: Depth-integrated down-canyon baroclinic M_2 energy flux for (a) *Feb09* and (b) *Apr09*. Vectors are plotted every grid point (250 m). The underlying colour is the energy flux magnitude. The black line is the smoothed canyon axis. Also shown are the locations of the moorings, Gooseneck Meander, and Butterfly Bowl.

the direction of the energy flux. Depth-integrated, the along-canyon energy flux around San Gregorio and Monterey Meanders is higher for *Feb09* than *Apr09* (Fig. 6a). However, this is simply a result of more baroclinic energy entering the canyon, rather than a difference due to standing/progressive waves. To quantify, the along-canyon energy flux integrated across the canyon mouth (Fig. 1a, line A) is 9 MW for *Feb09* and 6 MW for *Apr09*.

The vertical structure of the along-canyon energy flux between 15 km and the canyon head is markedly different for the two stratifications. There is an order 5 W m^{-2} near-bottom down-canyon energy flux between 10 km and 6 km for *Feb09* that is almost completely absent for *Apr09*. The vertical structure indicates a significant mode-2 component for *Feb09*, suggesting greater reflection and topographic scattering, while *Apr09* is dominated by a mode-1 internal tide propagating up-canyon.

Observed semidiurnal energy fluxes (black lines), calculated from the mooring data on yearday 56 and 86 (taken from Fig. 16 of Zhao et al., 2012), compare favourably with the two model simulations with respect to vertical structure. The energy fluxes at MP2, MP3, and LR4 on yearday 56 (pre-upwelling conditions) have a similar mode-2 structure and are down-canyon near-bottom, consistent with the *Feb09* model simulation. On yearday 86 (upwelling conditions), the energy fluxes from the same moorings have a dominant mode-1 structure and are up-canyon at all depths, consistent with the *Apr09* model simulation. Interestingly, both the observed and modelled energy fluxes have a dominant mode-1 structure at MP1 on yearday 56 (*Feb09*), suggesting that the partly standing wave may be restricted to the region between Gooseneck Meander and the canyon head.

To better visualise the spatial distribution of down-canyon energy fluxes in the upper canyon, the model energy flux is separated into up-canyon and down-canyon levels. At each model grid point, "down-canyon" is defined as the down-canyon direction along the smoothed canyon axis where the axis is nearest the grid point. Any sigma level at that grid point where the direction of the energy flux is within 45° of "down-canyon" is considered a down-canyon level.

The depth-integral of baroclinic M_2 energy flux on down-canyon levels is shown in Fig. 7. It is clear that down-canyon energy fluxes are more widespread for *Feb09* than *Apr09* and that the highest down-canyon energy fluxes are in the region between Gooseneck Meander and the canyon head. It is also evident that sampling the modelled internal tide field only at the mooring locations misses the majority of down-canyon energy energy fluxes.

4.3. Across-canyon energy flux

The transverse energy fluxes that are indicative of standing or partly standing waves are hard to diagnose in the canyon due to the meanders. The parallel/transverse decomposition is improved by using the smoothed canyon axis, but the across-canyon (transverse) component of the baroclinic M_2 energy flux is still dominated by deviations in the path of the internal tide beam from the path of the canyon axis. Nevertheless, there are higher depth-integrated across-canyon energy fluxes for *Feb09* than *Apr09* (Fig. 8a), particularly near Butterfly Bowl. Deflection of the internal tide beam into Butterfly Bowl has previously been noted by Hall and Carter (2011) for the *Feb09* model simulation. No such deflection of the internal tide beam is evident in plots of depth-integrated baroclinic M_2 energy flux for *Apr09* (not shown).

This is in agreement with the observed energy flux at LR4, the closest mooring to Butterfly Bowl. Zhao et al. (2012) showed that, during pre-upwelling conditions, the depth-integrated semidiurnal energy flux had a large across-canyon component into Butterfly Bowl. During upwelling conditions, the energy flux was directly up-canyon.

4.4. HKE, APE, and group speed

Energy density differences between the two stratifications are somewhat masked by differences in energy flux.

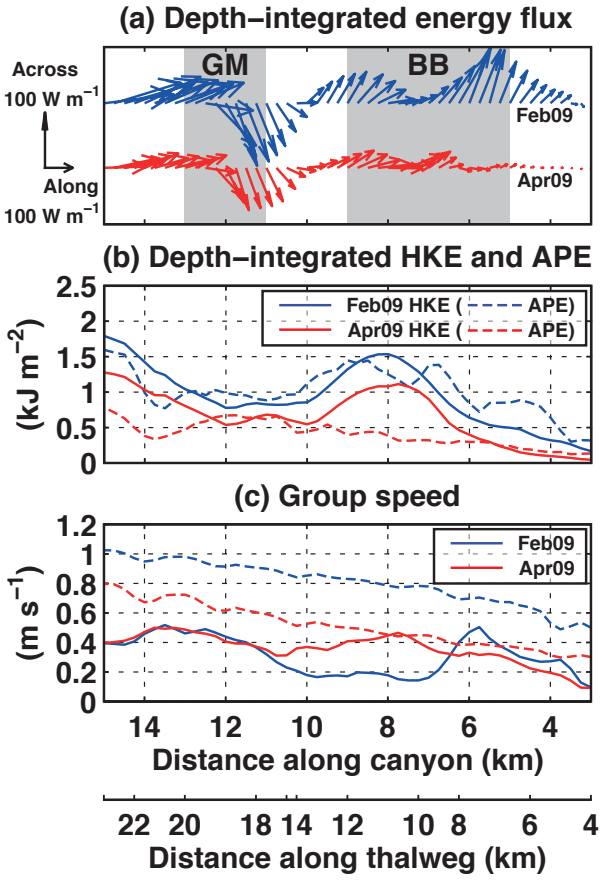

Figure 8: (a) Vectors of depth-integrated baroclinic M_2 energy flux with distance along the canyon for *Feb09* (blue) and *Apr09* (red). Across-canyon energy flux is exaggerated by a factor of two. The shaded areas are the locations of Gooseneck Meander and Butterfly Bowl. (b) Depth-integrated baroclinic M_2 HKE (solid lines) and APE (dashed lines) with distance along the canyon for the two model runs. (c) Model group speed (solid lines) and theoretical mode-1 group speed (dashed lines) for the two model runs.

Depth-integrated, both HKE and APE are higher for *Feb09* than *Apr09* (Fig. 8b), however, this is simply an effect of the higher depth-integrated energy flux. For *Feb09*, HKE and APE are approximately equal, HKE/APE is therefore around one, less than the theoretical value for a progressive internal wave, ~ 2.2. For *Apr09*, HKE is higher than APE at some locations (where HKE/APE is close to the theoretical value) and equal at others.

Differences between model internal wave group speed and theoretical mode-1 group speed are an indication of (partly) standing wave behaviour. $c_g^{\text{model}} < c_g^{\text{theory}}$ is expected for standing or partly standing waves (Martini et al., 2007) and is apparent for both *Feb09* and *Apr09* (Fig. 8c). However, the difference between model and theoretical group speed is a factor of two higher for the former.

5. Discussion: transition from partly standing to progressive waves

Previous analyses of standing and partly standing internal tides in MSC (Petruncio et al., 1998; Zhao et al., 2012) have identified the link to changes in stratification and proposed differences in internal tide reflection from bathymetry as a mechanism for the standing/progressive wave transition. Given that up-canyon internal tide energy fluxes have been observed at almost all locations in the canyon (e.g., Kunze et al., 2002; Carter and Gregg, 2002; Wain et al., Submitted), we can assume that the up-canyon propagating internal tide (generated on Sur Slope, outside the canyon mouth) is the major component of the partly standing wave. The down-canyon propagating internal tide after reflection from bathymetry (somewhere near the canyon head) is the minor component.

The reflective behaviour of normally incident internal waves approaching a sloping boundary from offshore can be predicted from α, the ratio of the topographic slope to the internal wave characteristic slope, $\alpha = s_{\text{topog}}/s_{\text{wave}}$. Topographic slope, $s_{\text{topog}} = \partial H/\partial \widetilde{x}$, where H is total depth and $\widetilde{x}$ is across-slope distance. If $\alpha < 1$ (subcritical) waves will be transmitted up the slope. If $\alpha > 1$ (supercritical) waves will be reflected back offshore. If $\alpha = 1$ (critical) linear theory breaks down, leading to nonlinear effects, wave breaking, and turbulent mixing (Eriksen, 1982; Ivey and Nokes, 1989; Dauxois et al., 2004). For obliquely incident internal waves, the effective topographic slope is less than the maximum topographic slope.

Petruncio et al. (1998) noted that increased stratification during ITEX2 flattened the internal tide characteristics, suggesting increasing down-canyon (supercritical) reflection from bathymetry near the canyon head. Similarly, Zhao et al. (2012) argued that the thalweg slope was supercritical to the semidiurnal internal tide during pre-upwelling conditions, suggesting down-canyon reflection from the canyon floor. During upwelling conditions, the thalweg slope was near-critical. This argument may be dependent on the path of the thalweg, as a meandering path will have a gentler topographic slope than a more direct (i.e., smoothed) path. Using the model stratification representative of pre-upwelling conditions (*Feb09*), the slope of the smoothed canyon axis (~ 0.04) is indeed supercritical to the M_2 internal tide ($\alpha > 1.5$) between 8 km and the canyon head, but near-critical farther down-canyon (Fig. 4a). Using the model stratification representative of upwelling conditions (*Apr09*), the smoothed canyon axis slope is almost entirely near-critical (Fig. 4b).

This two-dimensional view of MSC along the smoothed canyon axis is useful for diagnosing (partly) standing or progressive internal tides, but we need to view the canyon in three-dimensions to identify the area of bathymetry responsible for down-canyon reflection. The combined observational and model evidence suggests that the partly standing wave may be restricted to the region between Gooseneck Meander and the canyon head. Specifically,

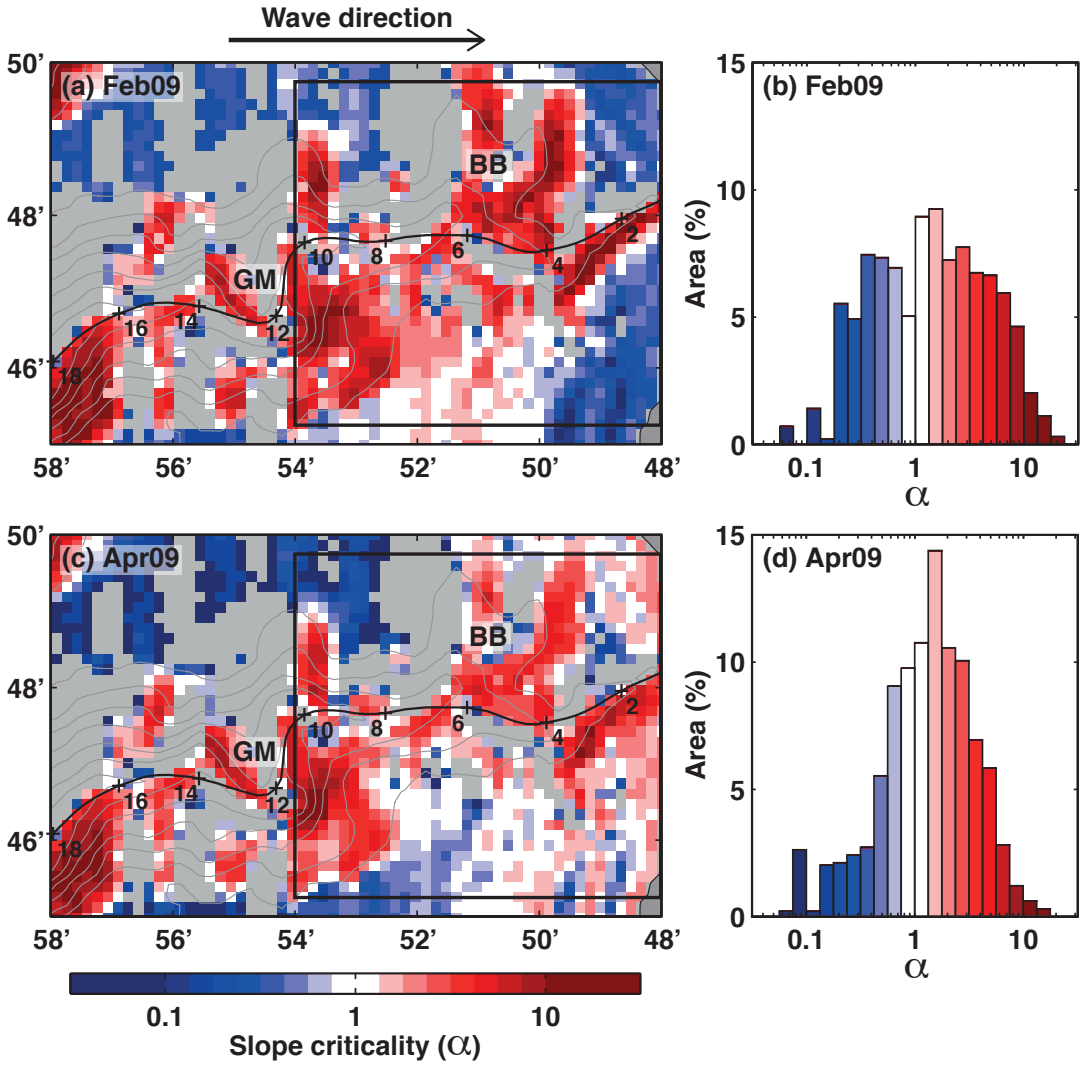

Figure 9: Bathymetric slope criticality to an M_2 internal tide propagating eastward (up-canyon) for (a) *Feb09* and (c) *Apr09* model stratifications (blue: subcritical, white: near-critical, red: supercritical). Grey indicates where the bathymetry deepens in the eastward direction and so cannot result in down-canyon supercritical reflection. Histograms of slope criticality by area in the region between Gooseneck Meander and the canyon head for (b) *Feb09* and (d) *Apr09*. The region is indicated by the black square in (a) and (c).

the low (< 1) HKE/APE ratio around 5 km for *Feb09* (Fig. 8b) may indicate that the reflective boundary responsible for the partly standing wave is proximate to this location.

Maps of bathymetric slope criticality to an M_2 internal tide (α) in the upper canyon region for both model stratifications are shown in Fig. 9a,c. As we are assuming the major component of the partly standing wave is propagating up-canyon (approximately eastward), α is calculated from the eastward component of topographic slope only (i.e., $\partial H/\partial x$). Only bathymetry that shallows in the eastward direction is considered as this is the orientation that can result in down-canyon supercritical reflection of an up-canyon propagating incident wave. Bathymetry that deepens in the eastward direction is shaded grey. In the upper canyon, small-scale meanders result in areas of steep canyon wall being oblique to the direction of internal tide propagation and it is clear that α is higher along these areas of canyon wall for *Feb09* than *Apr09*, especially near the canyon head (2-4 km).

Histograms of α in the region between Gooseneck Meander and the canyon head for both model stratifications are shown in Fig. 9b,d. Although the total area of supercritical slope in this region does not change significantly, there is a shift from strongly supercritical slopes for *Feb09* to weakly supercritical slopes for *Apr09*. To quantify, the area of strongly supercritical slope ($\alpha > 4$) decreases from 20% to 10%, while the area of weakly supercritical slope ($1.5 < \alpha < 4$) increases from 30% to 40%. Standing or partly standing internal waves are more likely to be setup by strongly supercritical, near-vertical boundaries.

This shift in slope criticality is a result of differences be-

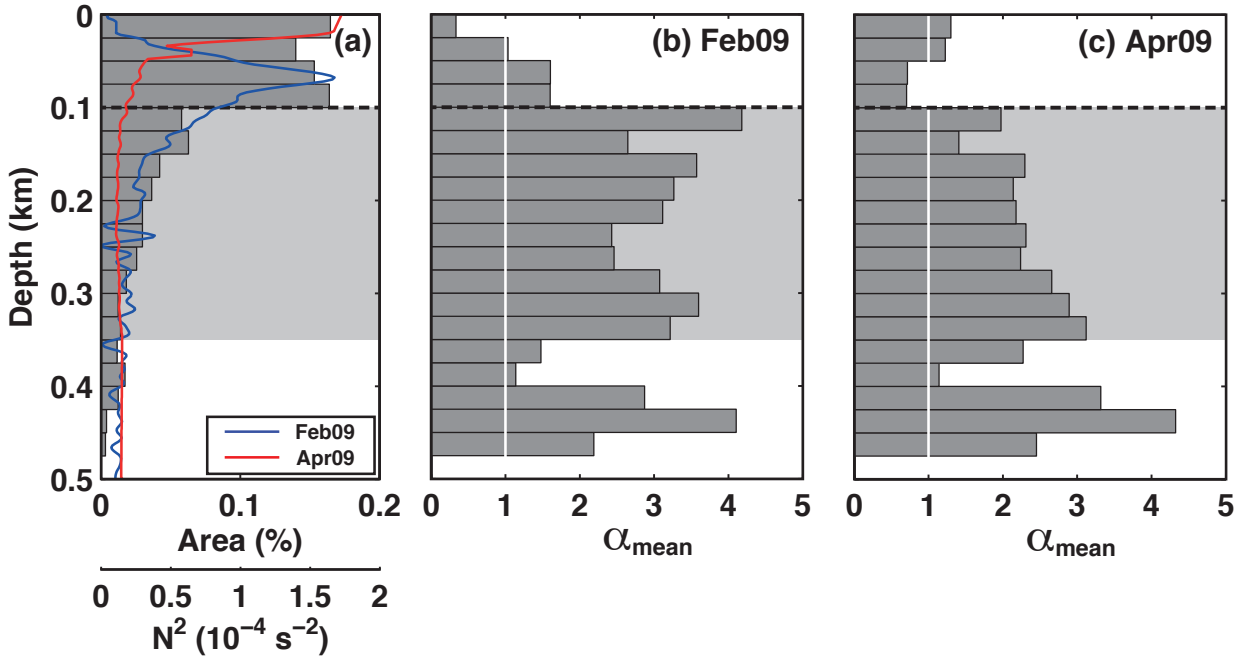

Figure 10: (a) Bathymetric area in 25-m depth bins for the region between Gooseneck Meander and the canyon head. The thick dashed line is the approximate depth of the canyon rim. The red and blue lines are N^2 profiles for *Feb09* and *Apr09* respectively. The 100-350 m depth-band, where N^2 below the canyon rim is higher for *Feb09* than *Apr09*, is shaded grey. Mean slope criticality in 25-m depth bins for (b) *Feb09* and (c) *Apr09* model stratifications. The white line is the critical value.

tween the model stratification profiles in the upper 350 m of the watercolumn (Fig. 10a). Although depth-averaged buoyancy frequency in the upper 350 m decreases slightly from 0.006 s^{-1} (*Feb09*) to 0.005 s^{-1} (*Apr09*), what is more important is the depth of maximum stratification relative to the depth of the canyon bathymetry. Hall et al. (2013) investigated the relationship between depth of stratification and depth of topography with respect to internal wave reflection and found that partially supercritical slopes reflect a similar fraction of internal wave energy as entirely supercritical slopes.

Here, the determining factor is the depth of maximum stratification relative to the depth of the canyon rim. From the distribution of bathymetric area with depth in the region between Gooseneck Meander and the canyon head (Fig. 10a), the canyon rim is $\sim$ 100 m deep. In the 100-350 m depth-band (shaded grey), N^2 is higher for *Feb09* than *Apr09* (up to 8×10^{-5} s^{-2} compared to $< 2 \times 10^{-5}$ s^{-2}) so the canyon floor and walls will be more supercritical to the M_2 internal tide for the former. This difference in slope criticality is evident from the mean of α in 25-m depth bins (Fig. 10b,c). α_{mean} is consistently higher for *Feb09* than *Apr09* in the 100-350 m depth-band. The effect most pronounced just below the canyon rim, with α typically twice as high for *Feb09* than *Apr09*.

For *Apr09*, the thin pycnocline in the upper 50 m of the watercolumn does not increase down-canyon reflection because it is above the canyon rim. It does, however, increase the criticality of the shelf region north and south of the canyon head. This region is subcritical for *Feb09* but near- and weakly supercritical for *Apr09* (Fig. 9a,c). Although the depth of maximum stratification is also above the canyon rim for *Feb09* ($\sim$ 70 m), the pycnocline is thick enough that it extends below the rim and increases down-canyon reflection from the canyon floor and walls. Thus, a small change in the depth of the pycnocline, if moved from below to above the canyon rim (or vice-versa), can have a dramatic effect on internal tide dynamics.

This mechanism also explains a down-canyon baroclinic M_2 energy flux west (seaward) of Gooseneck Meander that is apparent for both model runs (Fig. 7). Assuming this down-canyon energy flux is the result of supercritical reflection from the steep ridge within Gooseneck Meander, the topography is deeper ($>$ 400 m) than the depth of significant differences between the model stratification profiles, so no difference in reflection is expected.

Zhao et al. (2012) suggested that partly standing wave behaviour may be restricted to the region between Gooseneck Meander and the canyon head. This interpretation was based on an observed up-canyon, mode-1 internal tide energy flux and higher group speed at moored profiler MP1 (1.5 km down-canyon of the meander) during pre-upwelling conditions. However, these model simulations suggest the location of MP1 may not have been ideal for observing down-canyon energy fluxes (Fig. 7). For *Feb09*, down-canyon energy fluxes are almost as widespread in the region between Monterey and Gooseneck Meanders (not shown) as in the region between Gooseneck Meander

and the canyon head. In addition, *Feb09* pressure perturbation phase is spatially uniform between Monterey and Gooseneck Meanders (Fig. 5b), suggesting (partly) standing wave behaviour may occur farther down-canyon than observed.

6. Summary

Two previous studies, Petruncio et al. (1998) and Zhao et al. (2012), have observed a transition in the behaviour of the internal tide in the upper reaches of MSC from a standing or partly standing wave to a progressive wave. Both studies have attributed the transition to changes in stratification and internal tide reflection from bathymetry. Using a numerical model, we present evidence that either a partly standing or a progressive internal tide can be simulated in the canyon, simply by changing the initial stratification conditions in accordance with the observations.

The mechanism driving the transition is a dependence of down-canyon (supercritical) internal tide reflection from the canyon floor and walls on the depth of maximum stratification. If the main pycnocline is thick and extends below the canyon rim (e.g., pre-upwelling conditions), increased supercritical reflection of the up-canyon propagating internal tide back down the canyon sets up a partly standing wave between Gooseneck Meander and the canyon head. If the pycnocline is thin and above the canyon rim (e.g., upwelling conditions), decreased supercritical reflection allows the up-canyon progressive wave to dominate.

Acknowledgments

This work was funded by the National Science Foundation Grants OCE0751226 (University of Hawai'i) and OCE0751420 (University of Washington). Helpful comments on the manuscript were provided by two reviewers.

References

Alford, M. H., Zhao, Z., 2007. Global patterns of low-mode internal-wave propagation. Part II: Group velocity. Journal of Physical Oceanography 37, 1849–1858.

Baines, P. G., 1982. On internal tide generation models. Deep-Sea Research 29, 307–338.

Bell, T. H., 1975. Topographically-generated internal waves in the open ocean. Journal of Geophysical Research 80, 320–327.

Blumberg, A. F., Mellor, G. L., 1987. A description of a three-dimensional coastal ocean circulation model. In: Heaps, N. S. (Ed.), Three-Dimensional Coastal Ocean Models, Vol. 4. American Geophysical Union, Washington, D. C., pp. 1–16.

Carter, G. S., 2010. Barotropic and baroclinic M_2 tides in the Monterey Bay region. Journal of Physical Oceanography 40, 1766–1783.

Carter, G. S., Gregg, M. C., 2002. Intense, variable mixing near the head of Monterey Submarine Canyon. Journal of Physical Oceanography 32, 3145–3165.

Carter, G. S., Merrifield, M. A., 2007. Open boundary conditions for regional tidal simulations. Ocean Modelling 18, 194–209.

Dauxois, T., Didier, A., Falcon, E., 2004. Observations of near-critical reflection of internal waves in a stably stratified fluid. Physics of Fluids 16, 1936–1941.

Egbert, G. D., 1997. Tidal data inversion: interpolation and inference. Progress in Oceanography 40, 53–80.

Egbert, G. D., Erofeeva, S. Y., 2002. Efficient inverse modeling of barotropic ocean tides. Journal of Atmospheric and Oceanic Technology 19, 183–204.

Eriksen, C. C., 1982. Observations of internal wave reflection off sloping bottoms. Journal of Geophysical Research 87, 525–538.

Flather, R. A., 1976. A tidal model of the north-west European continental shelf. Memoires de la Societe Royale des Sciences de Liege 6, 141–164.

Gill, A. E., 1982. Atmosphere-Ocean Dynamics. Academic Press.

Gordon, R. L., Marshall, N. F., 1976. Submarine canyons: internal wave traps? Geophysical Research Letters 3, 622–624.

Gregg, M. C., Hall, R. A., Carter, G. S., Alford, M. H., Lien, R.-C., Winkel, D. P., Wain, D. J., 2011. Flow and mixing in Ascension, a steep, narrow canyon. Journal of Geophysical Research 116, C07016, doi:10.1029/2010JC006610.

Hall, R. A., Carter, G. S., 2011. Internal tides in Monterey Submarine Canyon. Journal of Physical Oceanography 41, 186–204.

Hall, R. A., Huthnance, J. M., Williams, R. G., 2013. Internal wave reflection on shelf slopes with depth-varying stratification. Journal of Physical Oceanography 43, 248–258.

Harris, P. T., Whiteway, T., 2011. Global distribution of large submarine canyons: Geomorphic differences between active and passive continental margins. Marine Geology 285, 69–86.

Hotchkiss, F. S., Wunsch, C., 1982. Internal waves in Hudson Canyon with possible geological implications. Deep-Sea Research 29, 415–442.

Ivey, G. N., Nokes, R. I., 1989. Vertical mixing due to the breaking of critical internal waves on sloping boundaries. Journal of Fluid Mechanics 204, 479–500.

Jachec, S. M., Fringer, O. B., Gerritsen, M. G., Street, R. L., 2006. Numerical simulation of internal tides and the resulting energetics within Monterey Bay and the surrounding area. Geophysical Research Letters 33, L12605, doi:10.1029/2006GL026314.

Johnston, T. M. S., Rudnick, D. L., Carter, G. S., Todd, R. E., Cole, S. T., 2011. Internal tidal beams and mixing near Monterey Bay. Journal of Geophysical Research 116, C03017, doi:10.1029/2010JC006592.

Kang, D., Fringer, O., 2012. Energetics of barotropic and baroclinic tides in the Monterey Bay Area. Journal of Physical Oceanography 42, 272–290.

Key, S. A., 1999. Internal tidal bores in the Monterey Canyon. Master's thesis, Naval Postgraduate School, Monterey, CA.

Kunze, E., MacKay, C., McPhee-Shaw, E. E., Morrice, K., Girton, J. B., Terker, S. R., 2012. Turbulent mixing and exchange with interior waters on sloping boundaries. Journal of Physical Oceanography 42, 910–927.

Kunze, E., Rosenfeld, L. K., Carter, G. S., Gregg, M. C., 2002. Internal waves in Monterey Submarine Canyon. Journal of Physical Oceanography 32, 1890–1913.

Lee, I.-H., Lien, R.-C., Liu, J. T., Chuang, W.-S., 2009. Turbulent mixing and internal tides in Gaoping (Kaoping) Submarine Canyon, Taiwan. Journal of Marine Systems 76, 383–396.

Lueck, R. G., Osborn, T. R., 1985. Turbulence measurements in a submarine canyon. Continental Shelf Research 4, 681–698.

Martini, K. I., Alford, M. H., Nash, J. D., Kunze, E., Merrifield, M. A., 2007. Diagnosing a partly standing internal wave in Mamala Bay, Oahu. Geophysical Research Letters 34, L17604, doi:10.1029/2007GL029749.

Nash, J. D., Alford, M. H., Kunze, E., 2005. Estimating internal wave energy fluxes in the ocean. Journal of Atmospheric and Oceanic Technology 22, 1551–1570.

Nash, J. D., Kunze, E., Lee, C. M., Sanford, T. B., 2006. Structure of the baroclinic tide generated at Kaena Ridge, Hawaii. Journal of Physical Oceanography 36, 1123–1135.

Nash, J. D., Kunze, E., Toole, J. M., Schmitt, R. W., 2004. Internal tide reflection and turbulent mixing on the continental slope. Journal of Physical Oceanography 34, 1117–1134.

Petruncio, E. T., Paduan, J. D., Rosenfeld, L. K., 2002. Numerical simulations of the internal tide in a submarine canyon. Ocean

Modelling 4, 221–248.
Petruncio, E. T., Rosenfeld, L. K., Paduan, J. D., 1998. Observations of the internal tide in Monterey Canyon. Journal of Physical Oceanography 28, 1873–1903.
Wain, D. J., Gregg, M. C., Alford, M. H., Lien, R.-C., Hall, R. A., Carter, G. S., Submitted. Propagation and dissipation of the internal tide in upper Monterey Canyon. Journal of Geophysical Research.
Wang, X., Chao, Y., Dong, C., Farrara, J., Li, Z., McWilliams, J. C., Paduan, J. D., Rosenfeld, L. K., 2009. Modeling tides in Monterey Bay, California. Deep-Sea Research II 56, 219–231.
Wang, Y. H., Lee, I.-H., Liu, J. T., 2008. Observation of internal tidal currents in the Kaoping Canyon off southwestern Taiwan. Estuarine, Coastal and Shelf Science 80, 153–160.
Wunsch, C., Webb, S., 1979. The climatology of deep ocean internal waves. Journal of Physical Oceanography 9, 235–243.
Zhao, Z., Alford, M. H., Lien, R.-C., Gregg, M. C., Carter, G. S., 2012. Internal tides and mixing in a submarine canyon with time-varying stratification. Journal of Physical Oceanography 42, 2121–2142.